

## Article

# Effect of Alkoxy Substituents on the Regioselectivity of Catalytic C-H Activation in Benzoic Acids: Experimental and DFT Study

Vladimir B. Kharitonov<sup>1</sup>, Dmitry V. Muratov<sup>1</sup> , Yulia V. Nelyubina<sup>1</sup>  and Dmitry A. Loginov<sup>1,2,\*</sup> 

<sup>1</sup> A. N. Nesmeyanov Institute of Organoelement Compounds, Russian Academy of Sciences, ul. Vavilova 28, 119991 Moscow, Russia

<sup>2</sup> Higher Engineering School "New Materials and Technologies", Plekhanov Russian University of Economics, 36 Stremyanny Per., 117997 Moscow, Russia

\* Correspondence: dloginov@ineos.ac.ru

**Abstract:** This work demonstrates the influence of the catalyst and alkyne nature on the regioselectivity of rhodium-catalyzed annulation of alkoxy-substituted benzoic acids (such as 3-methoxybenzoic, 3,4-dimethoxybenzoic, and piperonylic acids) with alkynes. Here, X-ray diffraction and DFT calculation data gave evidence that the observed regioselectivity is provided by both steric and coordination effects of methoxy groups. The latter is the result of weak non-covalent C-H...O interactions with the supporting ligand rather than with the rhodium atom. We believe that these results are also valid for other reactions of the C-H activation of methoxy-substituted arene compounds.

**Keywords:** C-H activation; homogeneous catalysis; isocoumarins; methoxy directing group; rhodium



**Citation:** Kharitonov, V.B.; Muratov, D.V.; Nelyubina, Y.V.; Loginov, D.A. Effect of Alkoxy Substituents on the Regioselectivity of Catalytic C-H Activation in Benzoic Acids: Experimental and DFT Study. *Catalysts* **2023**, *13*, 389. <https://doi.org/10.3390/catal13020389>

Academic Editors: Mohamed Mokhtar M. Mostafa, Tamer S. Saleh and Nesreen S. Ahmed

Received: 26 January 2023

Revised: 5 February 2023

Accepted: 8 February 2023

Published: 10 February 2023

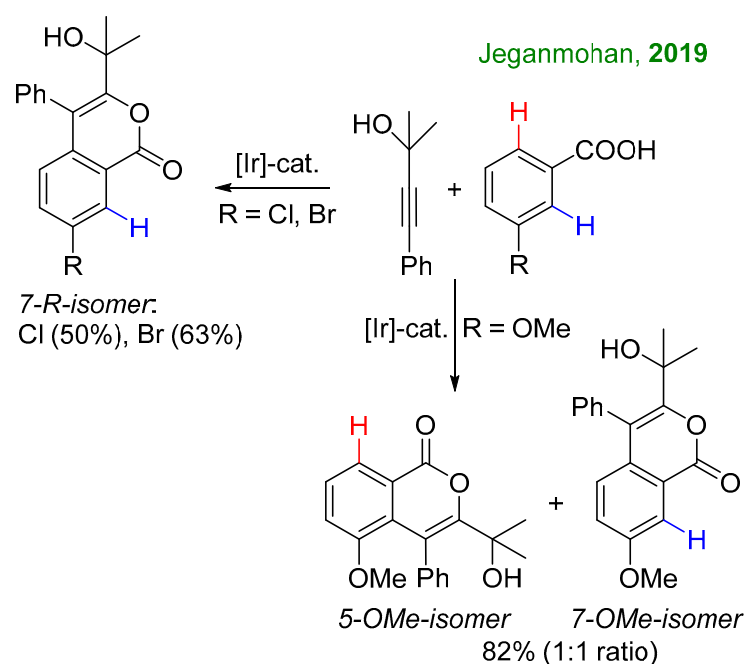


**Copyright:** © 2023 by the authors. Licensee MDPI, Basel, Switzerland. This article is an open access article distributed under the terms and conditions of the Creative Commons Attribution (CC BY) license (<https://creativecommons.org/licenses/by/4.0/>).

## 1. Introduction

Hydroxyl and alkoxy substituents are widely distributed in the structure of natural heterocyclic compounds [1,2]. Moreover, they are often responsible for diverse bioactivities, e.g., antibacterial and anticancer activity, and, therefore, are privileged pharmacophore groups. For example, hydroxy-substituted compounds account for more than 30% of all marketed drugs [3].

Transition metal-catalyzed annulation via the C-H activation process in arene or vinyl derivatives is a modern synthetic tool for the creation of heterocyclic compounds, including natural and pharmaceutical substances [4–8]. In particular, this approach allowed researchers to considerably improve the synthesis of the isocoumarin, isoquinoline, and indole alkaloids, such as spartolonin B [9], oxopalmatine [10], rosettacin [11,12], oxychelerythrine [13], and goniomitine [14], many of which contain hydroxyl or alkoxy groups. High selectivity is achieved through chelation with directing groups (carboxylic, hydroxamic, imine, etc.) [15–18]. Simple substituents without donor atoms, for example, alkyl, aryl, chlorine or bromine groups, in addition to steric effects, do not considerably affect the regioselectivity of C-H activation. At the same time, alkoxy groups are unique substituents that are not full-fledged directing groups, but contribute to the partial orientation of C-H activation to the *ortho*-position. For example, Sihag and Jeganmohan showed that annulations of 2-methyl-4-phenylbut-3-yn-2-ol with *meta*-Cl and *meta*-Br benzoic acids selectively afford only less sterically hindered 7-substituted isocoumarins, whereas a similar reaction with *meta*-OMe benzoic acid has poor regioselectivity, giving both 5- and 7-regioisomers in a 1:1 ratio (Scheme 1) [19]. Other researchers have also reported low selectivity for C-H activation of *meta*-OMe-substituted aryl compounds [20–25]. Interestingly, the formation of sterically unfavorable regioisomers has been observed for the formation of a naphthalene derivative from anisole or even *para*-OMe benzoic acid [26–28]. The exact reason for the poor regioselectivity of C-H activation of methoxy-substituted arenes was not clear until the present study.



**Scheme 1.** Iridium-catalyzed annulations of 2-methyl-4-phenylbut-3-yn-2-ol with *meta*-substituted benzoic acids [19]. Reaction conditions are as follows:  $[\text{Cp}^*\text{IrCl}_2]_2$  (3 mol%),  $\text{LiOAc}\cdot 2\text{H}_2\text{O}$  (1 equiv),  $\text{Ag}_2\text{CO}_3$  (1.1 equiv) in DCE at 80 °C for 20 h.

Herein we report an extensive study of the impact of the catalyst and alkyne nature on the regioselectivity of C-H activation of alkoxy-substituted benzoic acids, as well as the mechanistic aspects of these reactions based on X-ray and DFT studies.

## 2. Results and Discussion

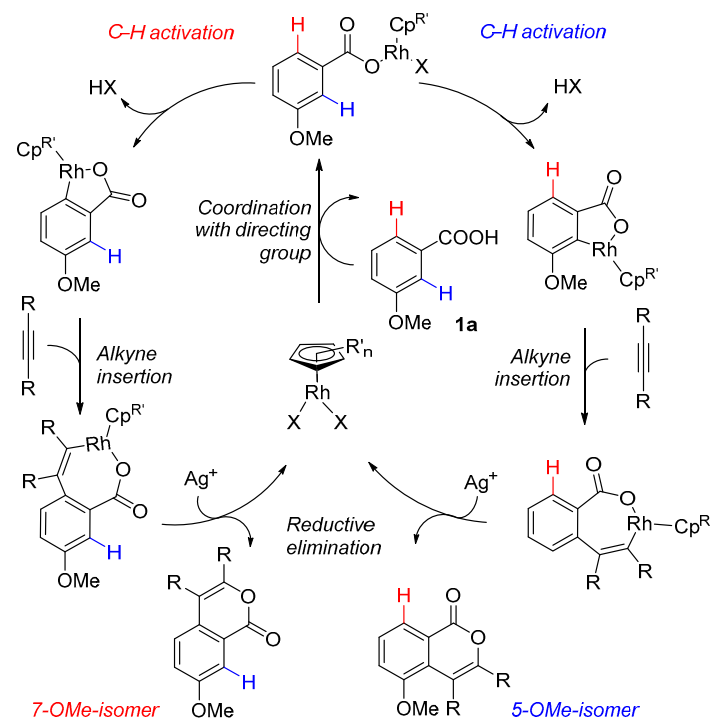
### 2.1. C-H Activation of 3-Methoxybenzoic Acid

First of all, to evaluate the influence of the catalyst nature on the regioselectivity of the C-H activation of 3-methoxybenzoic acid **1a**, we examined several rhodium complexes with different supporting ligands in the coupling reaction with diphenylacetylene **2a** (Table 1). Mild conditions were chosen, using  $\text{AgOAc}$  as the oxidant and methanol as the solvent at 80 °C [29–31]. It is noteworthy that an increase in the reaction temperature above 100 °C can lead to undesirable decarboxylation of **1a** [27,32–36]. We found that the use of rhodium complexes as catalysts with both electron-rich ( $\text{Cp}^*$  [37,38] and  $\text{Cp}^{\text{Ph}_3} = 1,2,4\text{-Ph}_3\text{-C}_5\text{H}_2$  [39]) and electron-deficient ( $\text{Cp}$  [40–42] and  $\text{Cp}^{\text{E}} = 1,3\text{-(COOEt)}_2\text{-C}_5\text{Me}_3$  [43]) cyclopentadienyl ligands leads to the preferential formation of the sterically unfavorable 5-substituted regioisomer **3aa** (entries 1–4), with the ratio of regioisomers being higher (up to 2.4:1) for the electron-rich ligands (entries 1 and 2 vs. 3 and 4). Most of the complexes demonstrated a high overall conversion (70–90%), while the  $[\text{Cp}^{\text{E}}\text{RhCl}_2]_2$  complex gave a mixture of **3aa** and **3aa'** with a total yield of only 20% (entry 4). The reduced catalytic activity of the latter is not clear, since electron-deficient ligands can facilitate C–H activation [44,45], which is usually the rate-determining step (for a conventional mechanism, see Scheme 2). It is believed that too many electron-withdrawing groups in the supporting ligand can also prevent with the reductive elimination step. Similar reactions with diethylacetylene **2b** also afforded mixtures of 5- and 7-methoxyisocoumarins **3ab**/**3ab'** (entries 5–8), but with a ratio of regioisomers close to 1:1. Moreover, in the case of the  $[\text{Cp}^{\text{E}}\text{RhCl}_2]_2$  complex the less sterically hindered 7-methoxyisocoumarin **3ab'** becomes predominant (entry 8). Thus, we can conclude that the regioselectivity of annulation of **1a** with alkynes depends not only on the supporting ligand, but also on the nature of the alkyne, which unambiguously suggests the importance of the alkyne insertion step for regioselectivity.

**Table 1.** Catalyst screening in the annulation of 3-methoxybenzoic acid **1a** with alkynes <sup>a</sup>.

Entry	R	Catalyst	Total Yield, % <sup>b</sup>	Ratio of 5/7-Isomers <sup>c</sup>
1	Ph	[Cp <sup>*</sup> RhCl <sub>2</sub> ] <sub>2</sub>	90	2.4:1
2	Ph	[Cp <sup>Ph3</sup> RhI <sub>2</sub> ] <sub>2</sub>	66	2.2:1
3	Ph	[CpRhI <sub>2</sub> ] <sub>n</sub>	91	1.85:1
4	Ph	[Cp <sup>E</sup> RhCl <sub>2</sub> ] <sub>2</sub>	20	1.72:1
5	Et	[Cp <sup>*</sup> RhCl <sub>2</sub> ] <sub>2</sub>	97	1.40:1
6	Et	[Cp <sup>Ph3</sup> RhI <sub>2</sub> ] <sub>2</sub>	97	1.25:1
7	Et	[CpRhI <sub>2</sub> ] <sub>n</sub>	94	1.10:1
8	Et	[Cp <sup>E</sup> RhCl <sub>2</sub> ] <sub>2</sub>	95	0.90:1

<sup>a</sup> Reaction conditions are as follows: 0.25 mmol (38 mg) of **1a**, 0.5 mmol of alkyne, 2.0 mol % (based on Rh) of the catalyst, 0.5 mmol (83 mg) of AgOAc, and methanol (2 mL) at 80 °C for 8 h. <sup>b</sup> Total yields are given after preliminary purification by column chromatography. <sup>c</sup> Regioisomeric ratios are determined by <sup>1</sup>H NMR spectroscopy.

**Scheme 2.** Two pathways for annulation of **1a** with alkynes.

All regioisomers **3aa/3aa'** and **3ab/3ab'** were separated and isolated individually using column chromatography. The structures of isocoumarins **3aa** and **3aa'** were determined by X-ray diffraction (Figures 1 and 2). In both cases, the symmetry-independent part of the unit cell contains two formula units. In **3aa**, the methoxy group is located in the plane of the isocoumarin fragment (the maximum value of dihedral angle C6-C5-O3-C9 is 4.5°), with the methyl substituent turning opposite to the incoming alkyne moiety in accordance

with a strong steric hindrance. In contrast, in the less sterically hindered isomer **3aa'**, the dihedral angle C6-C7-O3-C9 reaches  $22.4^\circ$ . The X-ray data suggests that the predominant formation of **3aa** should be provided by some additional coordination other than simple chelation of the carboxyl group.

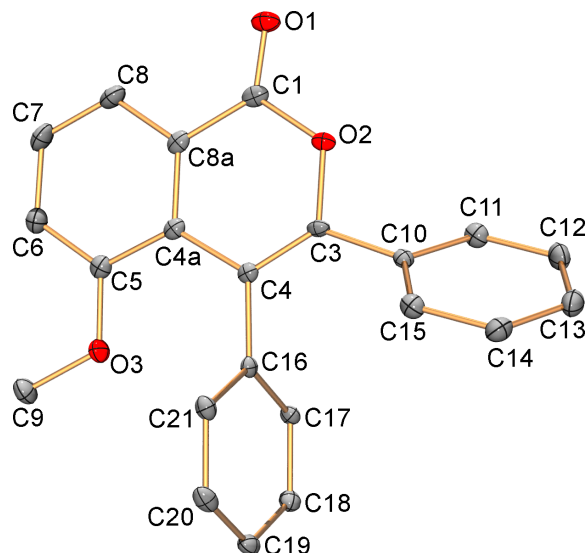


**Figure 1.** Structure of compound **3aa** (one of two symmetry-independent molecules). Ellipsoids are shown at the 50% level. Hydrogen atoms are omitted for clarity. Selected bond lengths (Å) for the first/second symmetry-independent species are as follows: C1–O1 1.206(1)/1.208(3), C1–O2 1.368(3)/1.370(3), C3–O2 1.387(3)/1.389(3), C5–O3 1.360(3)/1.356(3), C1–C8a 1.459(4)/1.454(4), C3–C4 1.336(4)/1.346(4), C4–C4a 1.465(4)/1.460(4), C4a–C8a 1.400(4)/1.408(4), C4a–C5 1.412(4)/1.419(4), C5–C6 1.382(4)/1.381(4), C6–C7 1.376(4)/1.386(4), C7–C8 1.377(4)/1.370(4), and C8–C8a 1.390(4)/1.389(4).

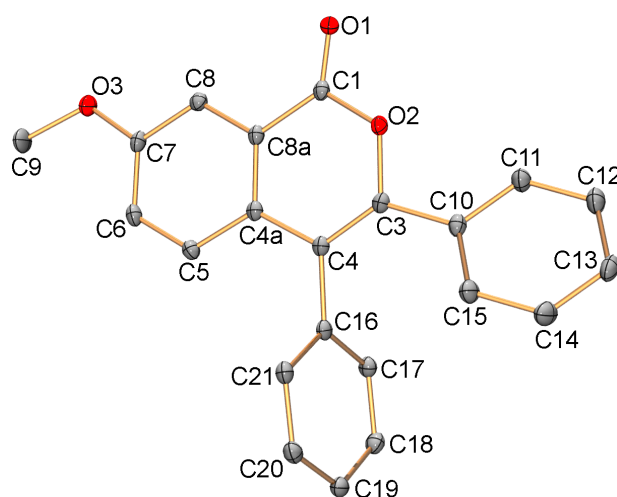
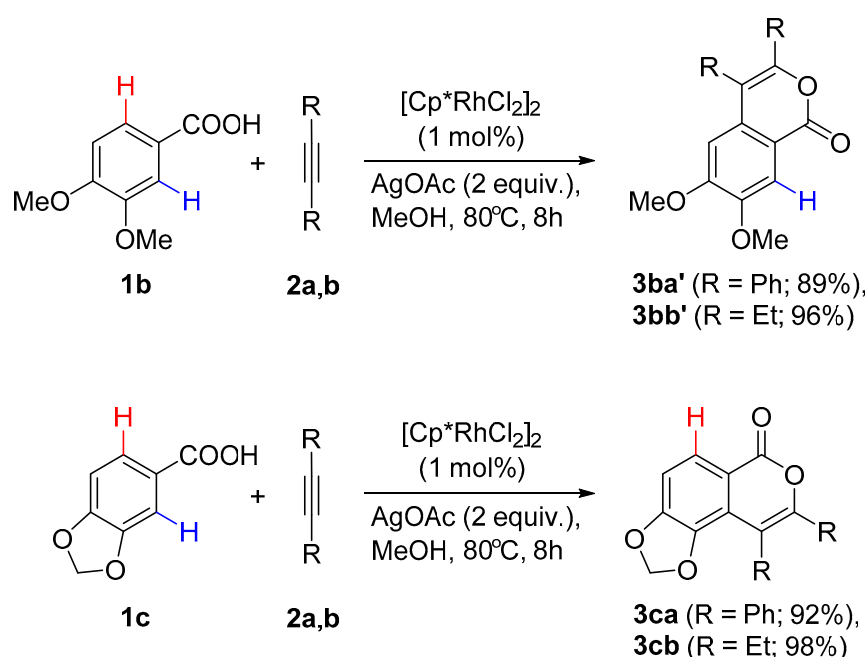


**Figure 2.** Structure of compound **3aa'** (one of two symmetry-independent molecules). Ellipsoids are shown at the 50% level. Hydrogen atoms are omitted for clarity. Selected bond lengths (Å) for the first/second symmetry-independent species are as follows: C1–O1 1.208(2)/1.198(2), C1–O2 1.371(2)/1.371(2), C3–O2 1.384(2)/1.393(2), C7–O3 1.363(2)/1.366(2), C1–C8a 1.462(3)/1.472(3), C3–C4 1.349(3)/1.352(3), C4–C4a 1.457(3)/1.462(3), C4a–C8a 1.400(3)/1.403(3), C4a–C5 1.405(3)/1.403(3), C5–C6 1.383(3)/1.382(3), C6–C7 1.396(3)/1.395(3), C7–C8 1.386(3)/1.386(3), and C8–C8a 1.392(3)/1.386(3).

## 2.2. C-H Activation of 3,4-Dimethoxybenzoic and Piperonylic Acids

To further emphasize the importance of both steric and coordination effects of the methoxy group, we involved 3,4-dimethoxybenzoic and piperonylic acids (**1b** and **1c**) in annulation with alkynes catalyzed by the  $[\text{Cp}^*\text{RhCl}_2]_2$  complex (Scheme 3). In each case, the reaction proceeds with excellent regioselectivity, giving only one of the two possible isomers. For example, annulation of **1b** with **2a,b** afforded the less sterically hindered isocoumarins **3ba'** and **3bb'** in accordance with steric control, which is provided by repulsion of two adjacent methoxy groups and shielding of one of two possible positions for C-H activation (see below). On the other hand, the reactions of **1c** selectively gave opposite regioisomeric isocoumarins **3ca** and **3cb** as a result of C-H activation of the position nearest to the ether substituent due to coordination control. In the case of reactions with diphenylacetylene **2a**, only *trans*-stilbene was isolated as a side product, which can be formed as a result of catalytic transfer hydrogenation by methanol [46,47].



**Scheme 3.** Rhodium-catalyzed annulations of **1b** and **1c** with alkynes.

The structures of isocoumarins **3ba'** and **3ca** were determined by X-ray diffraction (Figures 3 and 4). The symmetry-independent part of the unit cell for **3ba'** contains two formula units. The X-ray data for both independent molecules unambiguously confirm the shielding of the closest aromatic protons to methoxy groups, which prevents their C-H activation. On the contrary, from the structure of **3ca** it can be concluded that in the starting piperonylic acid **1c**, these positions are open to C-H activation.

## 2.3. DFT Investigation

The general mechanism of rhodium-catalyzed coupling of benzoic acids with alkynes has recently been investigated computationally by Nagashima and Tanaka [44]. They demonstrated that the use of electron-deficient supporting ligands, such as Cp and  $\text{Cp}^E$ , facilitates the C-H activation step, making alkyne insertion a rate-determining step. To explain the regioselectivity of C-H activation of 3-methoxybenzoic acid **1a**, we performed DFT calculations for these two key steps at the M06L(D3)/LANL2DZ level. Unexpectedly, in contrast to the parent benzoic acid, in the case of **1a**, the alkyne insertion has a considerably higher energy of the transition state than for C-H activation, not only for electron-deficient supporting ligands, but also for electron-rich ones ( $\text{Cp}^*$  and  $\text{Cp}^{\text{Ph}_3}$ ). For example, for the formation of both regioisomers in the case of the reaction catalyzed by  $[\text{Cp}^*\text{RhCl}_2]_2$ , the transition states of diphenylacetylene insertion  $\text{TS1\_T\_Cp}^*$  and  $\text{TS'1\_T\_Cp}^*$  have higher

Gibbs free energies (by ca. 8 kcal mol<sup>-1</sup>) than the transition states of the C-H activation TS0\_Cp\* and TS'0\_Cp\* (Figure 5). The same pattern was observed for the reaction with diethylacetylene, as well as for annulations catalyzed by all other rhodium complexes (see Supporting Information for energy profiles). It allows us to consider the transition state for the alkyne insertion as a rate-determining transition state [48]. At the same time, the C-H activation step still has the highest activation energy for annulations, with diphenylacetylene catalyzed by [Cp\*RhCl<sub>2</sub>]<sub>2</sub> and [Cp<sup>Ph</sup><sub>3</sub>RhI<sub>2</sub>]<sub>2</sub>. It is interesting to note that just these reactions provided the highest excess of the 5-methoxy regioisomer.

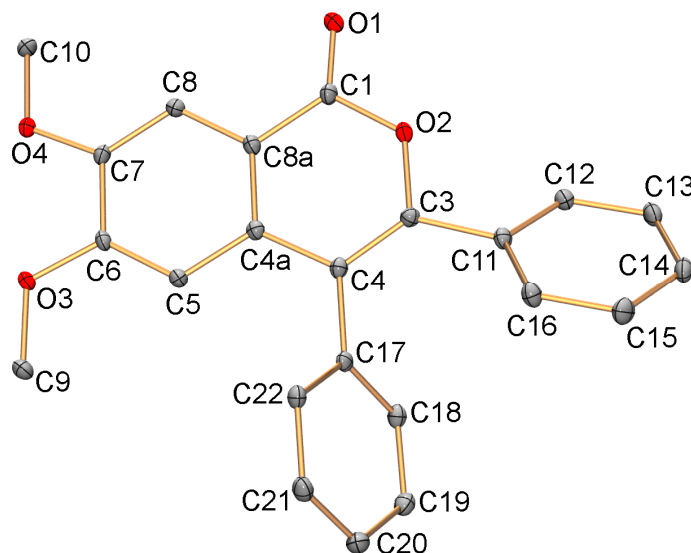


**Figure 3.** Structure of compound **3ba'** (one of two symmetry-independent molecules). Ellipsoids are shown at the 50% level. Hydrogen atoms are omitted for clarity. Selected bond lengths (Å) for the first/second symmetry-independent species are as follows: C1-O1 1.213(2)/1.211(2), C1-O2 1.3758(18)/1.3740(18), C3-O2 1.3888(19)/1.385(2), C6-O3 1.3557(18)/1.3583(18), C7-O4 1.3474(18)/1.3580(18), C1-C8a 1.448(2)/1.452(2), C3-C4 1.352(2)/1.349(2), C4-C4a 1.461(2)/1.463(2), C4a-C8a 1.396(2)/1.394(2), C4a-C5 1.408(2)/1.411(2), C5-C6 1.376(2)/1.381(2), C6-C7 1.421(2)/1.415(2), C7-C8 1.378(2)/1.376(2), and C8-C8a 1.406(2)/1.407(2).

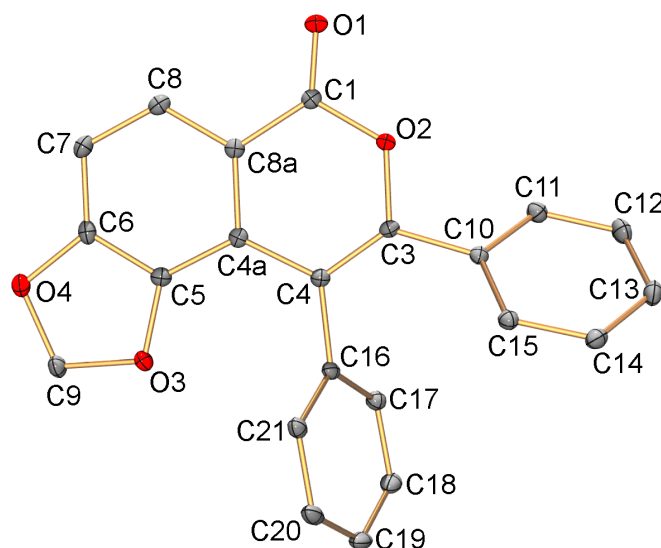


**Figure 4.** Structure of compound **3ca**. Ellipsoids are shown at the 50% level. Hydrogen atoms are

omitted for clarity. Selected bond lengths (Å) are as follows: C1-O1 1.2060(16), C1-O2 1.3742(16), C3-O2 1.3840(15), C5-O3 1.3719(16), C6-O4 1.3670(16), C1-C8a 1.4552(18), C3-C4 1.3470(18), C4-C4a 1.4588(18), C4a-C8a 1.4208(18), C4a-C5 1.3897(18), C5-C6 1.3852(19), C6-C7 1.3718(19), C7-C8 1.386(2), and C8-C8a 1.3969(19).

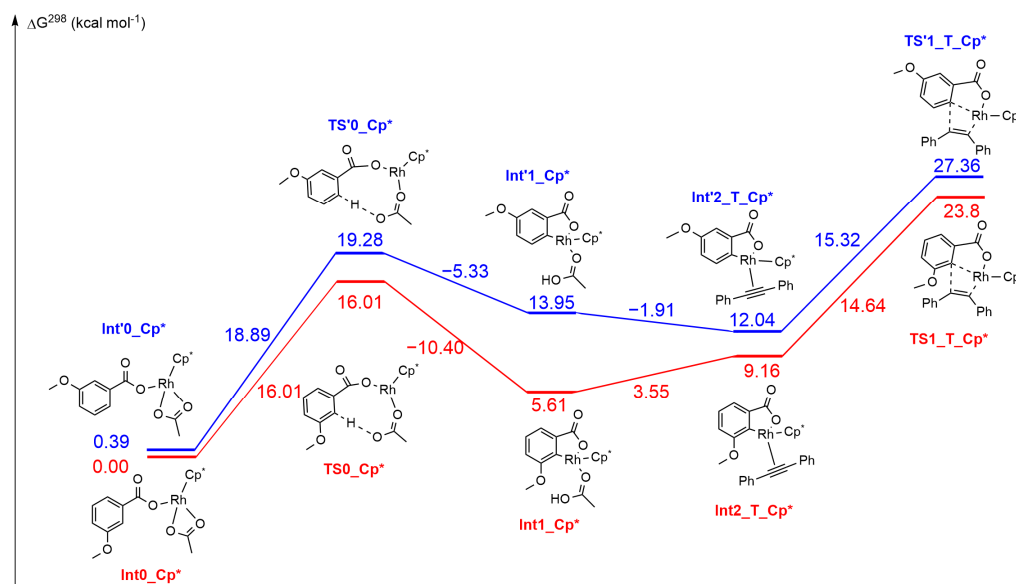


**Figure 5.** Energy profiles of C-H activation and alkyne insertion steps for the annulation of **1a** with diphenylacetylene catalyzed by  $[\text{Cp}^*\text{RhCl}_2]_2$ . The calculated Gibbs free energies are given relative to the **Int0\_Cp\*** intermediate at the M06L(D3)/LANL2DZ level with CPCM correction for methanol solvation (in  $\text{kcal}\cdot\text{mol}^{-1}$ , at 298 K).

Another important feature was found to be the lower energies of the intermediate and transition states for the pathway of formation of sterically unfavorable 5-OMe-regioisomers as compared with those for 7-OMe-regioisomers. The reaction with diethylacetylene catalyzed by  $[\text{Cp}^E\text{RhCl}_2]_2$  is the only exception (Figure 6), where the transition state for the 5-OMe-regioisomer **TS1\_H\_CpE** has a higher Gibbs free energy (by ca.  $0.4 \text{ kcal mol}^{-1}$ ) than for the 7-OMe-regioisomer **TS'1\_H\_CpE**. These theoretical data correlate well with the experimentally observed regioselectivity of the annulation of **1a** (see above).

However, the primary analysis of the optimized structures did not reveal covalent interactions of the methoxy group, which could provide stabilization of the 5-OMe-regioisomers. The maximum energy difference between the regioisomers (ca.  $7\text{--}8 \text{ kcal mol}^{-1}$ ) is observed for the first intermediates **Int'1** and **Int1**, where the latter is stabilized by an intramolecular classical hydrogen bond between the methoxy group and coordinated acetic acid, which is absent for the other intermediate and transition states (Figure 7). Therefore, we assumed that weaker stabilizing forces also exist. It is known that weak non-covalent interactions play a crucial role in organo and metal complex catalysis [49–51]. To search for weak non-covalent interactions, we performed the AIM analysis [52] for the transition states of both steps. It was found that there are weak  $\text{C-H}\cdots\text{O}$  interactions (the electron density at the bond critical points  $\rho(r)$  is less than  $0.01 \text{ e bohr}^{-3}$ ) between  $\text{CH}_3$  or  $\text{CH}$  moieties of the supporting ligand and the oxygen atom of the methoxy group, when this group is located close to the C-H activated site (for example, see Figure 8a), which makes the formation of 5-OMe-regioisomers more favorable. In the case of the reaction with diethylacetylene catalyzed by  $[\text{Cp}^E\text{RhCl}_2]_2$ , the observed reverse regioselectivity may be caused by additional  $\text{C-H}\cdots\text{O}$  interactions between the  $\text{CH}_2$  moiety of alkyne and the oxygen atoms of the ester groups of the  $\text{Cp}^E$  ligand at the second step (Figure 8b). The values of the Laplacian of the electron density  $\nabla^2\rho(r)$ , as well as the Cremer and Kraka energy density  $H(r)$ , are positive, which give evidence of the non-covalent nature of all these interactions [53,54].

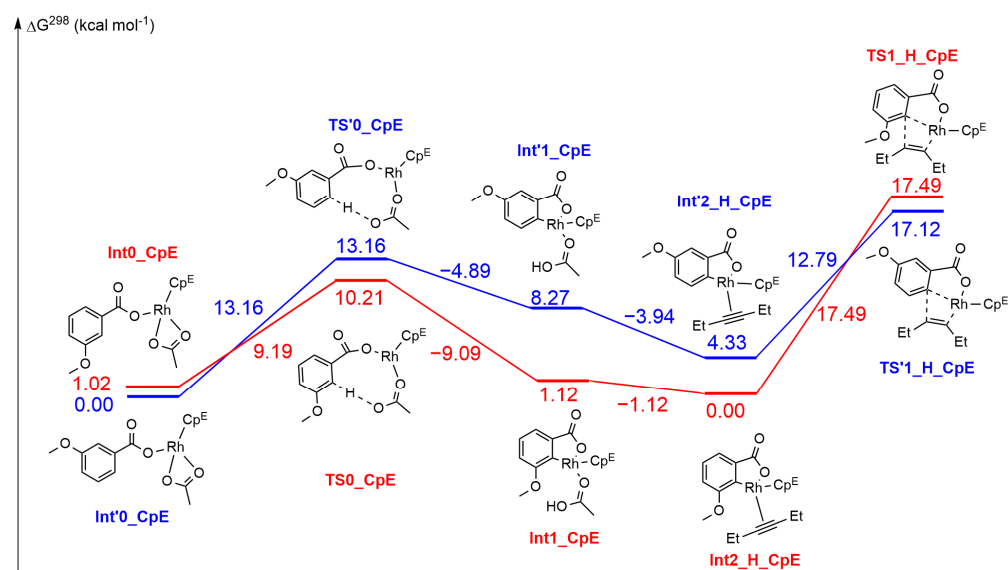


**Figure 6.** Energy profiles of C-H activation and alkyne insertion steps for the annulation of **1a** with diethylacetylene catalyzed by  $[\text{Cp}^{\text{E}}\text{RhCl}_2]_2$ . The calculated Gibbs free energies are given relative to the  $\text{Int}'0_{\text{CpE}}$  intermediate at the M06L(D3)/LANL2DZ level with CPCM correction for methanol solvation (in  $\text{kcal}\cdot\text{mol}^{-1}$ , at 298 K).

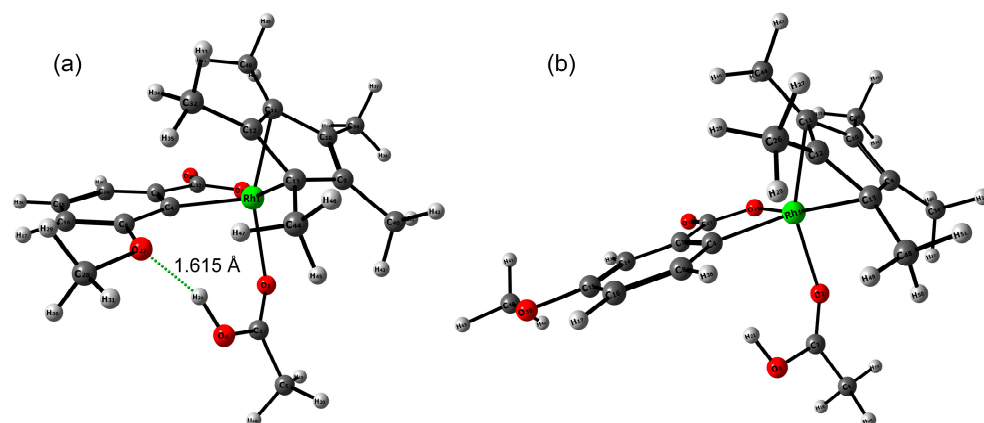


**Figure 7.** Intermediates  $\text{Int}1_{\text{Cp}^*}$  (a) and  $\text{Int}'1_{\text{Cp}^*}$  (b), optimized at the M06L(D3)/LANL2DZ level. The intramolecular distance  $\text{O}27 \cdots \text{H}21$  is equal to 1.615 Å.

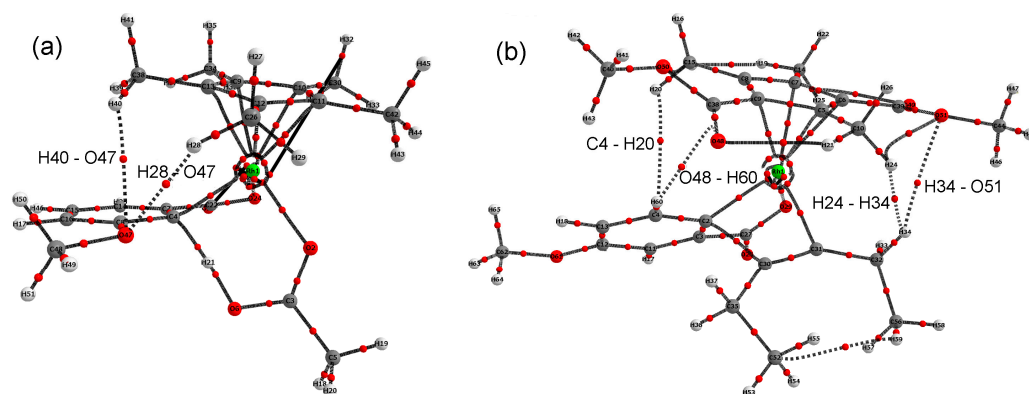


**Figure 8.** Theoretical molecular graphs of  $\text{TS}0_{\text{Cp}^*}$  (a) and  $\text{TS}'1_{\text{H}_{\text{CpE}}}$  (b). Calculated parameters

of the electron density distribution at the selected bond critical points are as follows: H40-O47 ( $\rho(r) = 0.008 \text{ e bohr}^{-3}$ ,  $\nabla^2\rho(r) = 0.035 \text{ e bohr}^{-3}$ ,  $H(r) = 0.002 \text{ a.u.}$ ); H28-O47 ( $\rho(r) = 0.007 \text{ e bohr}^{-3}$ ,  $\nabla^2\rho(r) = 0.030 \text{ e bohr}^{-3}$ ,  $H(r) = 0.002 \text{ a.u.}$ ); H34-O51 ( $\rho(r) = 0.005 \text{ e bohr}^{-3}$ ,  $\nabla^2\rho(r) = 0.018 \text{ e bohr}^{-3}$ ,  $H(r) = 0.001 \text{ a.u.}$ ).

### 3. Materials and Methods

#### 3.1. General Information

All catalytic reactions were carried out in air using distilled methanol. All other reagents were purchased from Acros or Aldrich and were used as received. Catalysts  $[\text{Cp}^*\text{RhCl}_2]_2$  [37],  $[\text{Cp}^{\text{Ph}_3}\text{RhI}_2]_2$  [39],  $[\text{CpRhI}_2]_n$  [40], and  $[\text{Cp}^{\text{E}}\text{RhCl}_2]_2$  [43] were prepared as described in the literature. Column chromatography was carried out using Macherey-Nagel silica gel 60 (particle size 0.04–0.063 mm) or neutral alumina. The  $^1\text{H}$  and  $^{13}\text{C}\{^1\text{H}\}$  NMR spectra were recorded on a Varian Inova 400 spectrometer operating at 400 and 101 MHz, respectively. Chemical shifts are given in ppm using residual solvent signals as internal standards. The HRMS spectra (ESI) were recorded on a TripleTOF 5600+ mass spectrometer (SCIEX).

#### 3.2. Reactions of 3-Methoxybenzoic Acid **1a** with Alkynes

3-Methoxybenzoic acid **1a** (38 mg, 0.25 mmol, 1 equiv), alkyne **2a** or **2b** (0.5 mmol, 2 equiv), the Rh complex (2.0 mol%), AgOAc (84 mg, 0.5 mmol, 2 equiv), and MeOH (2 mL) were placed in a Schlenk tube equipped with a stir bar. The reaction mixture was stirred at 80 °C for 8 h. After cooling, the formed precipitate was centrifuged off, the solvent was removed in vacuo, and the residue was chromatographed on silica (1 × 15 cm). The first colorless band containing unreacted alkyne was eluted with petroleum ether. The second (5-OMe-isomer) and third (7-OMe-isomer) bands were eluted with a mixture of petroleum ether and dichloromethane. In the case of reaction with diphenylacetylene **2a**, column chromatography should be repeated until complete separation of the regioisomers. Evaporation of the solvents gave the corresponding isocoumarins as colorless crystalline solids. Yields are given in Table 1.

5-Methoxy-3,4-diphenyl-1H-isochromen-1-one (**3aa**). Alkyne—diphenylacetylene **2a**. Eluent—petroleum ether/ $\text{CH}_2\text{Cl}_2$  (1:1).  $^1\text{H}$  NMR (400 MHz,  $\text{CDCl}_3$ )  $\delta$  8.03 (d,  $J = 7.9 \text{ Hz}$ , 1H), 7.46 (t,  $J = 8.0 \text{ Hz}$ , 1H), 7.23–7.18 (m, 5H), 7.17–7.09 (m, 6H), 3.32 (s, 3H).  $^{13}\text{C}\{^1\text{H}\}$  NMR (101 MHz,  $\text{CDCl}_3$ )  $\delta$  162.4, 156.3, 151.1, 137.8, 133.7, 130.8 (2C), 129.7 (2C), 129.2, 128.6, 127.8, 127.7 (2C), 127.5 (2C), 126.8, 122.2, 122.1, 117.7, 115.6, 56.1; HRMS (ESI)  $m/z$ — $[\text{M}+\text{H}]^+$  calculated for  $\text{C}_{22}\text{H}_{17}\text{O}_3$  329.1172, found—329.1178.

7-Methoxy-3,4-diphenyl-1H-isochromen-1-one (**3aa'**). Alkyne—diphenylacetylene **2a**. Eluent—petroleum ether/ $\text{CH}_2\text{Cl}_2$  (1:1).  $^1\text{H}$  NMR (400 MHz,  $\text{CDCl}_3$ )  $\delta$  7.81 (d,  $J = 2.7 \text{ Hz}$ , 1H), 7.41–7.39 (m, 2H), 7.34–7.28 (m, 2H), 7.26–7.10 (m, 8H), 3.93 (s, 3H).  $^{13}\text{C}\{^1\text{H}\}$  NMR (101 MHz,  $\text{CDCl}_3$ )  $\delta$  162.5, 159.6, 149.1, 134.6, 133.1 (2C), 132.7, 131.3, 129.19 (2C), 129.16 (2C), 128.8, 128.2, 128.0 (2C), 127.2, 124.3, 121.7, 116.9, 110.0, 56.0; HRMS (ESI)  $m/z$ — $[\text{M}+\text{H}]^+$  calculated for  $\text{C}_{22}\text{H}_{17}\text{O}_3$  329.1172, found—329.1178.

3,4-Diethyl-5-methoxy-1H-isochromen-1-one (**3ab**). Alkyne—diethylacetylene **2b**. Eluent—petroleum ether/ $\text{CH}_2\text{Cl}_2$  (3:1).  $^1\text{H}$  NMR (400 MHz,  $\text{CDCl}_3$ )  $\delta$  7.94 (d,  $J = 7.9 \text{ Hz}$ , 1H), 7.38 (t,  $J = 8.0 \text{ Hz}$ , 1H), 7.17 (d,  $J = 8.1 \text{ Hz}$ , 1H), 3.89 (s, 3H), 2.83 (q,  $J = 7.2 \text{ Hz}$ , 2H), 2.60 (q,  $J = 7.4 \text{ Hz}$ , 2H), 1.25 (t,  $J = 7.5 \text{ Hz}$ , 3H), 1.15 (t,  $J = 7.3 \text{ Hz}$ , 3H).  $^{13}\text{C}\{^1\text{H}\}$  NMR (101 MHz,  $\text{CDCl}_3$ )  $\delta$  163.1, 155.8, 154.3, 127.9, 124.3, 122.9, 122.0, 116.4, 113.4, 55.9, 24.2, 22.0, 15.6, 12.9; HRMS (ESI)  $m/z$ — $[\text{M}+\text{H}]^+$  calculated for  $\text{C}_{14}\text{H}_{17}\text{O}_3$  233.1178, found—233.1182.

3,4-Diethyl-7-methoxy-1H-isochromen-1-one (**3ab'**). Alkyne—diethylacetylene **2b**. Eluent—petroleum ether/ $\text{CH}_2\text{Cl}_2$  (3:1).  $^1\text{H}$  NMR (400 MHz,  $\text{CDCl}_3$ )  $\delta$  7.73 (d,  $J = 2.8 \text{ Hz}$ , 1H), 7.47 (d,  $J = 8.9 \text{ Hz}$ , 1H), 7.32 (dd,  $J = 8.9, 2.8 \text{ Hz}$ , 1H), 3.90 (s, 3H), 2.68–2.55 (m, 3H), 1.27 (t,  $J = 7.5 \text{ Hz}$ , 4H), 1.18 (t,  $J = 7.5 \text{ Hz}$ , 3H).  $^{13}\text{C}\{^1\text{H}\}$  NMR (101 MHz,  $\text{CDCl}_3$ )  $\delta$  163.3, 158.7, 153.1, 131.6, 124.4, 124.3, 122.1, 113.1, 110.3, 55.9, 24.0, 19.6, 14.6, 12.8; HRMS (ESI)  $m/z$ — $[\text{M}+\text{H}]^+$  calculated for  $\text{C}_{14}\text{H}_{17}\text{O}_3$  233.1178, found—233.1182.

### 3.3. Reactions of 3,4-Methoxybenzoic Acid **1b** with Alkynes

3,4-Methoxybenzoic acid **1b** (42 mg, 0.25 mmol, 1 equiv), alkyne (0.5 mmol, 2 equiv), complex  $[\text{Cp}^*\text{RhCl}_2]_2$  (1.5 mg, 1.0 mol%), AgOAc (84 mg, 0.5 mmol, 2 equiv), and MeOH (2 mL) were placed in a Schlenk tube equipped with a stir bar. The reaction mixture was stirred at 80 °C for 8 h. After cooling, the formed precipitate was centrifuged off, the solvent was removed in vacuo, and the residue was chromatographed on silica (1 × 15 cm). The first colorless band containing unreacted alkyne was eluted with petroleum ether. The second band was eluted with dichloromethane. Evaporation of the solvents gave isocoumarins **3ba'** or **3bb'** as colorless crystalline solids.

6,7-Dimethoxy-3,4-diphenyl-1H-isochromen-1-one (**3ba'**). Alkyne—diphenylacetylene **2a**. Yield—80 mg (89%).  $^1\text{H}$  NMR (400 MHz,  $\text{CDCl}_3$ )  $\delta$  7.77 (s, 1H), 7.46–7.39 (m, 3H), 7.33–7.26 (m, 4H), 7.23–7.15 (m, 3H), 6.57 (s, 1H), 4.01 (s, 3H), 3.74 (s, 3H).  $^{13}\text{C}\{^1\text{H}\}$  NMR (101 MHz,  $\text{CDCl}_3$ )  $\delta$  162.2, 154.9, 150.1, 149.7, 134.7, 134.5, 133.1, 131.2 (2C), 129.2 (2C), 129.1 (2C), 128.8, 128.2, 127.9 (2C), 116.8, 113.8, 109.5, 106.3, 56.4, 56.0; HRMS (ESI)  $m/z$ — $[\text{M}+\text{H}]^+$  calculated for  $\text{C}_{23}\text{H}_{19}\text{O}_4$  359.1283, found—359.1274.

3,4-Diethyl-6,7-dimethoxy-1H-isochromen-1-one (**3bb'**). Alkyne—diethylacetylene **2b**. Yield—63 mg (96%).  $^1\text{H}$  NMR (400 MHz,  $\text{CDCl}_3$ )  $\delta$  7.69 (s, 1H), 6.88 (s, 1H), 4.01 (s, 3H), 3.97 (s, 3H), 2.68–2.56 (m, 4H), 1.27 (t,  $J = 7.5$  Hz, 3H), 1.21 (t,  $J = 7.5$  Hz, 3H).  $^{13}\text{C}\{^1\text{H}\}$  NMR (101 MHz,  $\text{CDCl}_3$ )  $\delta$  163.0, 155.1, 154.3, 149.0, 133.6, 114.2, 112.9, 110.1, 103.6, 56.4, 56.3, 24.2, 19.7, 14.5, 12.8; HRMS (ESI)  $m/z$ — $[\text{M}+\text{H}]^+$  Calculated for  $\text{C}_{15}\text{H}_{19}\text{O}_4$  263.1283, found—263.1276.

### 3.4. Reactions of Piperonylic Acid **1c** with Alkynes

Piperonylic acid **1c** (41.5 mg, 0.25 mmol, 1 equiv), alkyne (0.5 mmol, 2 equiv), complex  $[\text{Cp}^*\text{RhCl}_2]_2$  (1.5 mg, 1.0 mol%), AgOAc (84 mg, 0.5 mmol, 2 equiv), and MeOH (2 mL) were placed in a Schlenk tube equipped with a stir bar. The reaction mixture was stirred at 80 °C for 8 h. After cooling, the formed precipitate was centrifuged off, the solvent was removed in vacuo, and the residue was chromatographed on silica (1 × 15 cm). The first colorless band containing unreacted alkyne was eluted with petroleum ether. The second band was eluted with dichloromethane. Evaporation of the solvents gave isocoumarins **3ca** or **3cb** as colorless crystalline solids.

8,9-Diphenyl-6H-[1,3]dioxolo [4,5-f]isochromen-6-one (**3ca**). Alkyne—diphenylacetylene **2a**. Yield—78 mg (91.5%).  $^1\text{H}$  NMR (400 MHz,  $\text{CDCl}_3$ )  $\delta$  8.08 (d, 1H), 7.32–7.24 (m, 7H), 7.21–7.14 (m, 3H), 7.02 (d,  $J = 8.3$  Hz, 1H), 5.80 (s, 2H).  $^{13}\text{C}\{^1\text{H}\}$  NMR (101 MHz,  $\text{CDCl}_3$ )  $\delta$  161.6, 153.3, 151.3, 142.7, 135.1, 133.0, 131.2 (2C), 129.4 (2C), 128.9, 128.1 (2C), 127.9, 127.8 (2C), 126.3, 122.0, 115.0, 113.5, 109.6, 102.1; HRMS (ESI)  $m/z$ — $[\text{M}+\text{H}]^+$  Calculated for  $\text{C}_{22}\text{H}_{15}\text{O}_4$  343.0971, found—343.0963.

8,9-Diethyl-6H-[1,3]dioxolo [4,5-f]isochromen-6-one (**3cb**). Alkyne—diethylacetylene **2b**. Yield—60 mg (98%).  $^1\text{H}$  NMR (400 MHz,  $\text{CDCl}_3$ )  $\delta$  7.96 (d,  $J = 8.3$  Hz, 1H), 6.94 (d,  $J = 8.4$  Hz, 1H), 6.11 (s, 2H), 2.69 (q,  $J = 7.4$  Hz, 2H), 2.56 (q,  $J = 7.5$  Hz, 2H), 1.25 (t,  $J = 7.5$  Hz, 3H), 1.14 (t,  $J = 7.4$  Hz, 3H).  $^{13}\text{C}\{^1\text{H}\}$  NMR (101 MHz,  $\text{CDCl}_3$ )  $\delta$  162.3, 154.9, 152.7, 141.4, 126.4, 122.5, 115.9, 111.3, 108.8, 101.9, 23.7, 20.8, 15.4, 12.7; HRMS (ESI)  $m/z$ — $[\text{M}+\text{H}]^+$  Calculated for  $\text{C}_{14}\text{H}_{15}\text{O}_2$  247.0971, found—247.0964.

### 3.5. X-ray Diffraction Study

The X-ray diffraction data were collected with a Bruker Quest D8 CMOS diffractometer using graphite monochromated Mo-K $\alpha$  radiation ( $\lambda = 0.71073$  Å,  $\omega$ -scans). Using Olex2 [55], the structures were solved with the ShelXT [56] structure solution program using intrinsic phasing and refined with the XL [57] refinement package using least-squares minimization against  $F^2$  in anisotropic approximation for non-hydrogen atoms. Positions of hydrogen atoms were calculated, and they were refined in the isotropic approximation in the riding model. Crystal data and structure refinement parameters are given in Table 2. Crystallographic data have been deposited with the Cambridge Crystallographic Data Centre as supplementary publications CCDC 2236072–2236075 and can be found in the Supplementary Materials.

**Table 2.** Crystal data and structure refinement parameters for **3aa**, **3aa'**, **3ba'**, and **3ca**.

	<b>3aa</b>	<b>3aa'</b>	<b>3ba'</b>	<b>3ca</b>
Formula unit	C <sub>22</sub> H <sub>16</sub> O <sub>3</sub>	C <sub>22</sub> H <sub>16</sub> O <sub>3</sub>	C <sub>23</sub> H <sub>18</sub> O <sub>4</sub>	C <sub>22</sub> H <sub>14</sub> O <sub>4</sub>
Molecular weight	328.35	328.35	358.37	342.33
Crystal system	Monoclinic	Triclinic	Monoclinic	Triclinic
Space group	<i>P</i> <sub>2</sub> <sub>1</sub> / <i>c</i>	<i>P</i> -1	<i>P</i> <sub>2</sub> <sub>1</sub> / <i>n</i>	<i>P</i> -1
<i>Z</i>	8	4	8	2
<i>a</i> (Å)	9.3656(9)	9.3355(2)	10.2837(5)	6.8314(2)
<i>b</i> (Å)	15.4672(19)	14.0312(4)	33.7768(15)	9.6009(2)
<i>c</i> (Å)	22.587(2)	14.1181(4)	10.3573(4)	12.8243(3)
$\alpha$ (deg)	90	60.4420(10)	90	71.7570(10)
$\beta$ (deg)	93.808(5)	87.511(2)	100.700(2)	79.6350(10)
$\gamma$ (deg)	90	82.039(2)	90	85.8540(10)
<i>V</i> (Å <sup>3</sup> )	3264.8(6)	1592.46(7)	3535.1(3)	785.69(3)
<i>D</i> <sub>calc</sub> (g cm <sup>-3</sup> )	1.336	1.370	1.347	1.447
Linear absorption $\mu$ (cm <sup>-1</sup> )	0.88	0.91	0.92	1.00
<i>F</i> (000)	1376	688	1504	356
$2\theta_{\max}$ (deg)	54	56	56	56
Reflections collected	34,022	19,932	27,437	9892
Independent reflections	6973	7685	8518	3782
Observed reflections ( <i>I</i> > 2 $\sigma$ ( <i>I</i> ))	3653	5218	6190	3027
Number of parameters	453	453	491	235
<i>R</i> <sub>1</sub>	0.0705	0.0575	0.0485	0.0415
<i>wR</i> <sub>2</sub>	0.1615	0.1499	0.1133	0.1034
GOOF	1.030	1.021	1.022	1.023
$\Delta\rho_{\max}/\Delta\rho_{\min}$ (e Å <sup>-3</sup> )	0.313/−0.235	0.541/−0.330	0.286/−0.235	0.305/−0.237

### 3.6. DFT Calculations

Geometry optimizations were performed using the ORCA program (version 5.0.3) [58] at the M06L(D3)/LANL2DZ [59] level with corrections for solvation in methanol (the CPCM model implemented in the Orca program). The optimized geometries were verified for one imaginary frequency for the transition states and none for the intermediate states. The AIM analysis of the electron density for the transition states was studied within Bader's atoms in molecules theory [52] using the AIMAll program packages [60].

## 4. Conclusions

In summary, we have shown that the rhodium-catalyzed annulation of 3-methoxybenzoic acid **1a** with alkynes results predominantly in the formation of sterically unfavorable 5-methoxyisocoumarins, with the ratio of regioisomers depending on the nature of the alkyne as well as the supporting ligand. The DFT calculations indicate that the favorable formation of 5-methoxy isomers is supported by weak non-covalent C–H···O interactions between the methoxy group and the supporting ligand. These secondary interactions can explain the high regioselectivity of the annulation of piperonylic acid **1c** with the formation of only angular isomers. On the contrary, the selective formation of distal regioisomers from 3,4-dimethoxybenzoic acid **1b** is provided by steric hindrance, resulting from the repulsion of two adjacent methoxy groups.

**Supplementary Materials:** The following supporting information can be downloaded at: <https://www.mdpi.com/article/10.3390/catal13020389/s1>, copies of NMR spectra, calculated energy profiles, optimized geometries, and theoretical molecular graphs.

**Author Contributions:** Conceptualization, D.A.L.; investigation, V.B.K.; NMR spectroscopy, D.V.M.; X-ray crystallography, Y.V.N.; writing—original draft preparation, D.A.L. and V.B.K.; writing—review and editing, D.A.L. and D.V.M. All authors have read and agreed to the published version of the manuscript.

**Funding:** This work was supported by the Russian Science Foundation (grant # 17-73-30036). The X-ray diffraction data were collected using the equipment of Center for Molecular Composition Studies of INEOS RAS with the financial support from the Ministry of Science and Higher Education of the Russian Federation (Contract/agreement No. 075-03-2023-642).

**Data Availability Statement:** Accession codes 2236075 (3aa), 2236073 (3aa'), 2236074 (3ba'), and 2236072 (3ca) contain the supplementary crystallographic data for this paper. These data can be obtained free of charge at [www.ccdc.cam.ac.uk/data\\_request/cif](http://www.ccdc.cam.ac.uk/data_request/cif) (accessed on 13 January 2023), or by emailing [data\\_request@ccdc.cam.ac.uk](mailto:data_request@ccdc.cam.ac.uk), or by contacting the Cambridge Crystallographic Data Centre, 12 Union Road, Cambridge CB2 1EZ, UK; Fax: +44-1223-336033.

**Acknowledgments:** D.A.L. is thankful to the Plekhanov Russian University of Economics for providing access to computation resources for DFT calculations.

**Conflicts of Interest:** The authors declare no conflict of interest.

## References

1. Shabir, G.; Saeed, A.; El-Seedi, H.R. Natural isocoumarins: Structural styles and biological activities, the revelations carry on . . . . *Phytochemistry* **2021**, *181*, 112568. [[CrossRef](#)]
2. Lichota, A.; Gwozdziński, K. Anticancer Activity of Natural Compounds from Plant and Marine Environment. *Int. J. Mol. Sci.* **2018**, *19*, 3533. [[CrossRef](#)] [[PubMed](#)]
3. Cramer, J.; Sager, C.P.; Ernst, B. Hydroxyl Groups in Synthetic and Natural-Product-Derived Therapeutics: A Perspective on a Common Functional Group. *J. Med. Chem.* **2019**, *62*, 8915–8930. [[CrossRef](#)] [[PubMed](#)]
4. Kharitonov, V.B.; Muratov, D.V.; Loginov, D.A. Cyclopentadienyl complexes of group 9 metals in the total synthesis of natural products. *Coord. Chem. Rev.* **2022**, *471*, 214744. [[CrossRef](#)]
5. Jardim, G.A.M.; de Carvalho, R.L.; Nunes, M.P.; Machado, L.A.; Almeida, L.D.; Bahou, K.A.; Bower, J.F.; da Silva Júnior, E.N. Looking deep into C-H functionalization: The synthesis and application of cyclopentadienyl and related metal catalysts. *Chem. Commun.* **2022**, *58*, 3101–3121. [[CrossRef](#)]
6. Loginov, D.A.; Konoplev, V.E. Oxidative coupling of benzoic acids with alkynes: Catalyst design and selectivity. *J. Organomet. Chem.* **2018**, *867*, 14–24. [[CrossRef](#)]
7. Song, G.; Li, X. Substrate activation strategies in rhodium(III)-catalyzed selective functionalization of arenes. *Acc. Chem. Res.* **2015**, *48*, 1007–1020. [[CrossRef](#)]
8. Satoh, T.; Miura, M. Oxidative coupling of aromatic substrates with alkynes and alkenes under rhodium catalysis. *Chem. Eur. J.* **2010**, *16*, 11212–11222. [[CrossRef](#)]
9. Wang, Y.; Wang, C.; Wang, Y.; Dong, L.; Sun, J. Total synthesis of Sparstolonin B, a potent anti-inflammatory agent. *RSC Adv.* **2015**, *5*, 12354–12357. [[CrossRef](#)]
10. Li, X.; Huang, T.; Song, Y.; Qi, Y.; Li, L.; Li, Y.; Xiao, Q.; Zhang, Y. Co(III)-catalyzed annulative vinylene transfer via C-H activation: Three-step total synthesis of 8-oxopseudopalmitine and oxopalmitine. *Org. Lett.* **2020**, *22*, 5925–5930. [[CrossRef](#)]
11. Song, L.; Tian, G.; Van der Eycken, E.V. Rhodium(III)-catalyzed intermolecular cascade annulation through CH activation: Concise synthesis of rosettacin. *Mol. Catal.* **2018**, *459*, 129–134. [[CrossRef](#)]
12. Xu, X.; Liu, Y.; Park, C.-M. Rhodium(III)-catalyzed intramolecular annulation through C-H activation: Total synthesis of (±)-antofine, (±)-septicine, (±)-tylophorine, and rosettacin. *Angew. Chem. Int. Ed.* **2012**, *51*, 9372–9376. [[CrossRef](#)]
13. Jayakumar, J.; Parthasarathy, K.; Cheng, C.-H. One-pot synthesis of isoquinolinium salts by rhodium-catalyzed C-H bond activation: Application to the total synthesis of oxychelerythrine. *Angew. Chem. Int. Ed.* **2012**, *51*, 197–200. [[CrossRef](#)] [[PubMed](#)]
14. Zhou, B.; Du, J.; Yang, Y.; Li, Y. Rhodium(III)-catalyzed intramolecular redoxneutral annulation of tethered alkynes: Formal total synthesis of (±)-goniomitine. *Chem. Eur. J.* **2014**, *20*, 12768–12772. [[CrossRef](#)] [[PubMed](#)]
15. Carvalho, R.L.; Almeida, R.G.; Murali, K.; Machado, L.A.; Pedrosa, L.F.; Dolui, P.; Maiti, D.; da Silva Júnior, E.N. Removal and modification of directing groups used in metal-catalyzed C-H functionalization: The magical step of conversion into 'conventional' functional groups. *Org. Biomol. Chem.* **2021**, *19*, 525–547. [[CrossRef](#)] [[PubMed](#)]
16. Murali, K.; Machado, L.A.; Carvalho, R.L.; Pedrosa, L.F.; Mukherjee, R.; da Silva Júnior, E.N.; Maiti, D. Decoding directing groups and their pivotal role in C-H activation. *Chem. Eur. J.* **2021**, *27*, 12453–12508. [[CrossRef](#)]
17. Sambiagio, C.; Schönbauer, D.; Blicek, R.; Dao-Huy, T.; Pototschnig, G.; Schaaf, P.; Wiesinger, T.; Zia, M.F.; Wencel-Delord, J.; Besset, T.; et al. A comprehensive overview of directing groups applied in metal-catalysed CH functionalisation chemistry. *Chem. Soc. Rev.* **2018**, *47*, 6603–6743. [[CrossRef](#)]
18. Drapeau, M.P.; Goossen, L.J. Carboxylic acids as directing groups for C-H bond functionalization. *Chem. Eur. J.* **2016**, *22*, 18654–18677. [[CrossRef](#)]
19. Sihag, P.; Jeganmohan, M. Regioselective Synthesis of Isocoumarins via Iridium(III)-Catalyzed Oxidative Cyclization of Aromatic Acids with Propargyl Alcohols. *J. Org. Chem.* **2019**, *84*, 2699–2712. [[CrossRef](#)]
20. Luo, F.; He, S.; Gou, Q.; Chen, J.; Zhang, M. Rhodium-catalyzed oxidative coupling of benzoic acids with propargyl alcohols: An efficient access to isocoumarins. *Tetrahedron Lett.* **2021**, *64*, 152724. [[CrossRef](#)]
21. Vorobyeva, D.V.; Petropavlovskikh, D.A.; Godovikov, I.A.; Nefedov, S.E.; Osipov, S.N. Rh(III)-Catalyzed C-H Activation/Annulation of Aryl Hydroxamates with CF<sub>3</sub>-Containing  $\alpha$ -Propargyl  $\alpha$ -Amino Acid Derivatives. *Eur. J. Org. Chem.* **2021**, *2021*, 1883–1890. [[CrossRef](#)]

22. Kudo, E.; Shibata, Y.; Yamazaki, M.; Masutomi, K.; Miyauchi, Y.; Fukui, M.; Sugiyama, H.; Uekusa, H.; Satoh, T.; Miura, M.; et al. Oxidative Annulation of Arenecarboxylic and Acrylic Acids with Alkynes under Ambient Conditions Catalyzed by an Electron-Deficient Rhodium(III) Complex. *Chem. Eur. J.* **2016**, *22*, 14190–14194. [[CrossRef](#)] [[PubMed](#)]
23. Hyster, T.K.; Rovis, T. Rhodium(III)-Catalyzed C–H Activation Mediated Synthesis of Isoquinolones from Amides and Cyclopropenes. *Synlett* **2013**, *24*, 1842–1844. [[CrossRef](#)] [[PubMed](#)]
24. Unoh, Y.; Hirano, K.; Satoh, T.; Miura, M. Synthesis of highly substituted isocoumarins by rhodium-catalyzed annulation of readily available benzoic acids. *Tetrahedron* **2013**, *69*, 4454–4458. [[CrossRef](#)]
25. Chinnagolla, R.K.; Jegannathan, M. Regioselective synthesis of isocoumarins by ruthenium-catalyzed aerobic oxidative cyclization of aromatic acids with alkynes. *Chem. Commun.* **2012**, *48*, 2030–2032. [[CrossRef](#)]
26. Kharitonov, V.B.; Muratov, D.V.; Nelyubina, Y.V.; Loginov, D.A. Formation of a Naphthalene Framework by Rhodium(III)-Catalyzed Double C–H Functionalization of Arenes with Alkynes: Impact of a Supporting Ligand and an Acid Additive. *Synthesis* **2022**, *54*, 5119–5127.
27. Inai, Y.; Usuki, Y.; Satoh, T. Synthesis of Benzo-Fused Cyclic Compounds via Rhodium-Catalyzed Decarboxylative Coupling of Aromatic Carboxylic Acids with Alkynes. *Synthesis* **2021**, *53*, 3029–3036.
28. Honjo, Y.; Shibata, Y.; Kudo, E.; Namba, T.; Masutomi, K.; Tanaka, K. Room Temperature Decarboxylative and Oxidative [2+2+2] Annulation of Benzoic Acids with Alkynes Catalyzed by an Electron-Deficient Rhodium(III) Complex. *Chem. Eur. J.* **2018**, *24*, 317–321. [[CrossRef](#)]
29. Kharitonov, V.B.; Runikhina, S.A.; Nelyubina, Y.V.; Muratov, D.V.; Chusov, D.; Loginov, D.A. Easy Access to Versatile Catalytic Systems for C–H Activation and Reductive Amination Based on Tetrahydrofluorenyl Rhodium(III) Complexes. *Chem. Eur. J.* **2021**, *27*, 10903–10912. [[CrossRef](#)]
30. Datsenko, V.P.; Nelyubina, Y.V.; Smol'yakov, A.F.; Loginov, D.A. Cyclooctadiene iridium complexes [Cp\*Ir(COD)X]<sup>+</sup> (X = Cl, Br, I): Synthesis and application for oxidative coupling of benzoic acid with alkynes. *J. Organomet. Chem.* **2018**, *874*, 7–12. [[CrossRef](#)]
31. Frasco, D.A.; Lilly, C.P.; Boyle, P.D.; Ison, E.A. Cp\*Ir<sup>III</sup>-Catalyzed Oxidative Coupling of Benzoic Acids with Alkynes. *ACS Catal.* **2013**, *3*, 2421–2429. [[CrossRef](#)]
32. Arsenov, M.A.; Fedorov, Y.V.; Muratov, D.V.; Nelyubina, Y.V.; Loginov, D.A. Synthesis of isocoumarins and PAHs with electron-withdrawing substituents: Impact of the substituent nature on the photophysical behavior. *Dye. Pigment.* **2022**, *206*, 110653. [[CrossRef](#)]
33. Arsenov, M.A.; Loginov, D.A. Recent Advances in the Synthesis of Isocoumarins and Polyaromatic Hydrocarbons for Photoactive Materials. *INEOS OPEN* **2021**, *4*, 133–139. [[CrossRef](#)]
34. Molotkov, A.P.; Arsenov, M.A.; Kapustin, D.A.; Muratov, D.V.; Shepel', N.E.; Fedorov, Y.V.; Smol'yakov, A.F.; Knyazeva, E.I.; Lypenko, D.A.; Dmitriev, A.V.; et al. Effect of Cp-Ligand Methylation on Rhodium(III)-Catalyzed Annulations of Aromatic Carboxylic Acids with Alkynes: Synthesis of Isocoumarins and PAHs for Organic Light-Emitting Devices. *ChemPlusChem* **2020**, *85*, 334–345. [[CrossRef](#)] [[PubMed](#)]
35. Vinogradov, M.M.; Loginov, D.A. Rhoda- and iridacarborane halide complexes: Synthesis, structure and application in homogeneous catalysis. *J. Organomet. Chem.* **2020**, *910*, 121135. [[CrossRef](#)]
36. Loginov, D.A.; Muratov, D.V.; Nelyubina, Y.V.; Laskova, J.; Kudinov, A.R.  $\mu$ -Borole triple-decker complexes as catalysts for oxidative coupling of benzoic acid with alkynes. Structure of a hybrid rhodacyclopentadienyl/borole triple-decker complex. *J. Mol. Catal. A* **2017**, *426*, 393–397. [[CrossRef](#)]
37. White, C.; Yates, A.; Maitlis, P.M. ( $\eta^5$ -Pentamethylcyclopentadienyl)Rhodium and -Iridium Compounds. *Inorg. Synth.* **1992**, *29*, 228–234.
38. Ueura, K.; Satoh, T.; Miura, M. Rhodium- and Iridium-Catalyzed Oxidative Coupling of Benzoic Acids with Alkynes via Regioselective C–H Bond Cleavage. *J. Org. Chem.* **2007**, *72*, 5362–5367. [[CrossRef](#)]
39. Kharitonov, V.B.; Muratov, D.V.; Nelyubina, Y.V.; Shutkov, I.A.; Nazarov, A.A.; Loginov, D.A. Triphenylcyclopentadienyl Rhodium Complexes in Catalytic C–H Annulations. Application for Synthesis of Natural Isocoumarins. *J. Org. Chem.* **2023**. [[CrossRef](#)]
40. Loginov, D.A.; Vinogradov, M.M.; Starikova, Z.A.; Petrovskii, P.V.; Kudinov, A.R. Arene complexes  $[(\eta\text{-C}_5\text{H}_5)\text{M}(\eta\text{-C}_6\text{R}_6)]^{2+}$  (M = Rh, Ir). *Russ. Chem. Bull.* **2004**, *53*, 1949–1953. [[CrossRef](#)]
41. Loginov, D.A.; Belova, A.O.; Kudinov, A.R. Rhodacarboranes as catalysts for oxidative coupling of benzoic acid with diphenylacetylene. *Russ. Chem. Bull.* **2014**, *63*, 983–986. [[CrossRef](#)]
42. Lin, W.; Li, W.; Lu, D.; Su, F.; Wen, T.-B.; Zhang, H.-J. Dual Effects of Cyclopentadienyl Ligands on Rh(III)-Catalyzed Dehydrogenative Arylation of Electron-Rich Alkenes. *ACS Catal.* **2018**, *8*, 8070–8076. [[CrossRef](#)]
43. Shibata, Y.; Tanaka, K. Catalytic [2+2+1] Cross-Cyclootrimerization of Silylacetylenes and Two Alkynyl Esters To Produce Substituted Silylfulvenes. *Angew. Chem. Int. Ed.* **2011**, *50*, 10917–10921. [[CrossRef](#)] [[PubMed](#)]
44. Nagashima, Y.; Ishigaki, S.; Tanaka, J.; Tanaka, K. Acceleration Mechanisms of C–H Bond Functionalization Catalyzed by Electron-Deficient CpRh(III) Complexes. *ACS Catal.* **2021**, *11*, 13591–13602. [[CrossRef](#)]
45. Araujo Dias, A.J.; Takahashi, H.; Nogami, J.; Nagashima, Y.; Tanaka, K. Oxidative [4 + 2] annulation of 1-naphthols with alkynes accelerated by an electron-deficient rhodium(III) catalysts. *Org. Biomol. Chem.* **2022**, *20*, 1008–1012. [[CrossRef](#)]
46. Wang, D.; Astruc, D. The Golden Age of Transfer Hydrogenation. *Chem. Rev.* **2015**, *115*, 6621–6686. [[CrossRef](#)]
47. Biriukov, K.O.; Afanasyev, O.I.; Godovikova, M.I.; Loginov, D.A.; Chusov, D.A. Osmium-catalyzed reduction processes. *Russ. Chem. Rev.* **2022**, *91*, RCR5045. [[CrossRef](#)]

48. Kozuch, S.; Martin, J.M.L. The Rate-Determining Step is Dead. Long Live the Rate-Determining State! *ChemPhysChem* **2011**, *12*, 1413–1418. [[CrossRef](#)]
49. Mahmudov, K.T.; Gurbanov, A.V.; Guseinov, F.I.; Guedes da Silva, M.F.C. Noncovalent interactions in metal complex catalysis. *Coord. Chem. Rev.* **2019**, *387*, 32–46. [[CrossRef](#)]
50. Mahmudov, K.T.; Kopylovich, M.N.; Guedes da Silva, M.F.C.; Pombeiro, A.J.L. (Eds.) *Noncovalent Interactions in Catalysis*; Royal Society of Chemistry: Cambridge, UK, 2019.
51. MacMillan, D.W.C. The advent and development of organocatalysis. *Nature* **2008**, *455*, 304–308. [[CrossRef](#)]
52. Bader, R.F.W. *Atoms in Molecules: A Quantum Theory*; Oxford University Press: Oxford, UK, 1990.
53. Kumar, N.; Saha, S.; Sastry, G.N. Towards developing a criterion to characterize non-covalent bonds: A quantum mechanical study. *Phys. Chem. Chem. Phys.* **2021**, *23*, 8478–8488. [[CrossRef](#)]
54. Cremer, D.; Kraka, E. A Description of the Chemical Bond in Terms of Local Properties of Electron Density and Energy. *Croat. Chem. Acta* **1984**, *56*, 1259–1281.
55. Dolomanov, O.V.; Bourhis, L.J.; Gildea, R.J.; Howard, J.A.K.; Puschmann, H. OLEX2: A complete structure solution, refinement and analysis program. *J. Appl. Cryst.* **2009**, *42*, 339–341. [[CrossRef](#)]
56. Sheldrick, G.M. SHELXT—Integrated space-group and crystal-structure determination. *Acta Cryst.* **2015**, *71 Pt A*, 3–8. [[CrossRef](#)]
57. Sheldrick, G.M. A short history of SHELX. *Acta Cryst.* **2008**, *64 Pt A*, 112–122. [[CrossRef](#)]
58. Neese, F. Software update: The ORCA program system—Version 5.0. *WIREs Comput. Mol. Sci.* **2022**, *12*, e1606. [[CrossRef](#)]
59. Zhao, Y.; Truhlar, D.G. A new local density functional for main-group thermochemistry, transition metal bonding, thermochemical kinetics, and noncovalent interactions. *J. Chem. Phys.* **2006**, *125*, 194101. [[CrossRef](#)]
60. Keith, T.A. *AIMAll*, Version 19.10.12; TK Gristmill Software: Overland Park, KS, USA, 2019. Available online: [aim.tkgristmill.com](http://aim.tkgristmill.com) (accessed on 12 February 2021).

**Disclaimer/Publisher's Note:** The statements, opinions and data contained in all publications are solely those of the individual author(s) and contributor(s) and not of MDPI and/or the editor(s). MDPI and/or the editor(s) disclaim responsibility for any injury to people or property resulting from any ideas, methods, instructions or products referred to in the content.